




Electrochemical properties of $\text{Na}_{0.5}\text{Bi}_{0.5}\text{TiO}_3$ perovskite as an anode material for sodium ion batteries

K. Kamala Bharathi^{1,2,*} , Brindha Moorthy³, Hanuma Kumar Dara⁴, Lignesh Durai¹, and Do Kyung Kim^{3,*}

¹Department of Physics and Nanotechnology, SRM Institute of Science and Technology, Kattankulathur, Chennai 603203, India

²Nanotechnology Research Center (NRC), SRM Institute of Science and Technology, Kattankulathur, Chennai 603203, India

³Department of Materials Science and Engineering, Korea Advanced Institute of Science and Technology (KAIST), 291 Daehak-ro, Yuseong-gu, Daejeon 34141, Republic of Korea

⁴Advanced Magnetic Materials Laboratory, Department of Physics, Indian Institute of Technology Madras, Chennai 600036, India

Received: 15 February 2019

Accepted: 5 July 2019

© Springer Science+Business Media, LLC, part of Springer Nature 2019

ABSTRACT

Sodium ion batteries (SIBs) are possible low-cost alternative to the current lithium ion batteries and hold great perspectives for large-scale renewable energy storage. However, the unavailability of appropriate anode material hinders the practical application of SIBs. Herein, we have examined the structural and electrochemical properties of perovskite $\text{Na}_{0.5}\text{Bi}_{0.5}\text{TiO}_3$ (NBTO) and explored the possibilities of utilizing it as an anode component for Na ion batteries. The electrochemical measurement shows that the perovskite NBTO exhibits high sodium storage capability via alloying/de-alloying reaction, fast sodium storage kinetics, and a good cyclability. The perovskite $\text{Na}_{0.5}\text{Bi}_{0.5}\text{TiO}_3$ delivers a high capacity of $\sim 470 \text{ mAh g}^{-1}$ at 100 mA g^{-1} and 230 mAh g^{-1} at 250 mA g^{-1} , emerging as a new anode for SIBs. Furthermore, the perovskite $\text{Na}_{0.5}\text{Bi}_{0.5}\text{TiO}_3$ can retain a capacity of $\sim 215 \text{ mAh g}^{-1}$ after 50 cycles at 100 mA g^{-1} , which is comparable to several previous metal oxide anodes. In addition, the sodium storage behavior is investigated by ex situ XRD and XPS techniques. The high capacity and good rate capability suggest that the perovskite $\text{Na}_{0.5}\text{Bi}_{0.5}\text{TiO}_3$ has great potential to serve as anodes for high-performing SIBs.

K. Kamala Bharathi and Brindha Moorthy have contributed equally to this work.

Address correspondence to E-mail: kamalabharathi.k@ktr.srmuniv.ac.in; dkkim@kaist.ac.kr

<https://doi.org/10.1007/s10853-019-03834-9>

Published online: 15 July 2019

Introduction

Energy storage technology has attained a great leap in past three decades with the help of Li ion batteries (LIBs) [1–5]. LIBs are widely used in electronic and electrical devices such as mobile phones, laptops, electrical vehicles (EVs), etc [6, 7]. However, LIBs have a drawback due to the rarity of Li in earth, when a large-scale production is considered. In order to overcome the limitations due to the Li scarcity, a new material which is abundant in nature should be proposed as a replacement and as a key to gear up the energy storage technology. Sodium (Na), which is an abundant element on the earth, can be a strong technical replacement for the Li ion in the battery technology. Electrochemically Na is a material with a similar chemistry as of Li. Moreover, it has redox potential of ~ 2.71 V, which portrait it as a very promising candidate for replacement against Lithium [8]. Sodium ion batteries (SIBs) can be a potential replacement for LIBs in small-scale productions as well as in large-scale productions for energy storage applications [9, 10]. The anode materials used in LIBs, i.e., graphite cannot be employed as an anode for the SIBs due to its structural instability with Na [11]. Some of the anode materials that have been examined by various research groups around the globe are metals, metal oxides and metal sulfides-based conversion reaction anodes [12, 13]. Metal oxide-based anode materials exhibit high capacity, i.e., more than 500 mAh g^{-1} , but the capacity fading and high-volume expansions affect the process and efficiency [14–16]. For example, Fe_2O_3 , a transition metal oxide anode is observed with a reversible capacity of 386 mAh g^{-1} initially and found to be stable at 100 mAh g^{-1} over 200 cycles with an oversized current-density of 5 A g^{-1} [17]. Similarly, a high initial capacity of 580 mAh g^{-1} has been reported for the SnO thick films but the subsequent capacity fading is also reported. On the other hand, Sb-based anode materials exhibit moderate and stable capacity [18]. Likewise, the metal sulfides are also studied as an alternative anode material for SIBs. The large volume expansion in those metal sulfide anodes degrades the performance of the battery, which is another drawback [19, 20]. Apart from the transition metal oxide-based anode materials, N-doped porous carbon nanofibers are reported to have a discharge capacity of 152 mAh g^{-1} with considerably high capacity

retention even after 200 cycles [21]. The hard carbon for SIBs are reported to exhibit highest reversible capacity anode material with more than 300 mAh g^{-1} capacity at 0.1C rate even after 120 cycles [22]. Yet, the low capacity of carbonaceous anode hinders the practical application. But the graphene elements in the hard carbon and metal oxides contributed to a large extend toward rate capability [23].

A promising approach to overcome the volume expansion in alloying/de-alloying anodes in LIBs involves utilization of perovskite-based insertion hosts [24]. However, the capability of perovskite materials toward sodium ion storage is still mostly unexplored. Utilization of perovskite anodes can favorably develop a high capacity and stable sodium ion anode [25]. $\text{Na}_{0.5}\text{Bi}_{0.5}\text{TiO}_3$ (NBTO) is a well-known relaxor ferroelectric material, which undergoes a phase transitions from cubic to tetragonal structure at 673–773 K and then finally to rhombohedral structures at 5–528 K [26, 27]. On the process of invading a new anode material for SIBs with high capacity and high stability, we have examined the structural and electrochemical properties of NBTO perovskite oxide for the first time. The present study is aimed on the systematic examination of growth and electrochemical properties of NBTO bulk material prepared by a simple solid-state reaction and explore the potentials of utilizing them as an anode material for SIBs.

The sodium storage ability of NBTO perovskite is attractive with high capacity (470 mAh g^{-1} at 100 mA g^{-1}), good rate performance (50 mAh g^{-1} at 2 A g^{-1}) along with good stability. Furthermore, in order to identify the sodium storage mechanism in NBTO perovskite, the changes in the crystal structure, oxidation states of metal and oxygen ions are evaluated via the ex situ XRD, X-ray photoelectron spectroscopy (XPS) characterizations and ac impedance spectroscopy. The current research could trigger the utilization of other perovskite toward sodium ion storage.

Experimental methods

Synthesis of $\text{Na}_{0.5}\text{Bi}_{0.5}\text{TiO}_3$ perovskite material

The solid-state reaction method was employed to synthesis NBTO bulk material. The precursors used

in this process were of analytical grade. bismuth (III) oxide (Bi_2O_3), titanium dioxide (TiO_2) and sodium carbonate (Na_2CO_3) were weighed and then ground in a mortar pestle for 1 h. The homogenized powder collected after the grinding was pressed into pellet and then sintered at 850 °C for 5 h in tube furnace. The sintered pellet was ground again for 1 h, and final sintering was done at 1100 °C for 3 h to obtain the NBTO perovskite bulk material.

Characterization of NBTO perovskite material

The structural properties of synthesized NBTO perovskite material were studied in detail using Cu K_α ($\lambda = 0.15406$ nm) X-ray diffractometer (XRD, Rigaku, D/MAX-IIIC X-ray diffractometer, Tokyo, Japan). The morphological information and structural details of the material were studied employing field-emission scanning electron microscope (FE-SEM Philips XL30 FEG, Eindhoven, Netherland). The structural characterization of the material was understood with help of the Raman spectroscopy by employing a HR 800 Raman spectrophotometer (Jobin–Yvon–Horiba, France) which uses monochromatic He–Ne Laser (632.8 nm), operating at 20 mW.

Electrochemical characterization

The electrochemical studies were carried out using CR2032 coin cells. The slurry preparation is the essential process for fabricating an electrode which can be employed in CR2032 for electrochemical studies. NBTO powder was mixed CNT with the weight ratio of 80:20 before being used for electrochemical characterization. Commercially purchased multi-walled carbon nanotubes MWCNTs (Sigma-Aldrich) were used in this study to improve the electrochemical performance of NBT anode. The slurry was prepared by mixing $\text{Na}_{0.5}\text{Bi}_{0.5}\text{TiO}_3$ with carbon nanotubes (CNT)/ketjen black and teflonized acetylene black binder under the ratio of 80:10:10, and the slurry was coated on copper foil with a mass loading of $\sim 1.5\text{--}2$ mg cm^{-2} . The electrode was dried for 12 h in vacuum oven without any interruption, and then, the foil was cut into 12-mm-diameter electrode using the crimping tool without any disturbance in the surface. For the cell preparation, Na metal foil was cut with identical diameter specification as done with NBTO-coated electrode and

employed as an anode for the half-cell. Mixture of 1 M NaClO_4 solution and $\text{CH}_3\text{C}_2\text{H}_3\text{O}_2\text{CO}$ (propylene carbonate) with 2% of fluoroethylene carbonate was prepared, which was utilized as a liquid electrolyte of the cell through which the ionic conduction is possible. In order to avoid shorting between two electrodes, borosilicate fiber was used as the separator. The coin cell fabrication was carried out in the glove box with argon gas atmosphere. The cyclic voltammetry (CV) measurements were carried out with the help of Biologic Science Instruments (Model: VMP3) under the voltage window range from 0.01 to 3 V. The charge/discharge between 0.01 and 3 V at different C rates were measured by employing the VMP3 Biologic potentiostat.

Results and discussion

Figure 1a shows the Rietveld refined XRD pattern of NBTO bulk material. NBTO is seen to crystallize in pure $R3C$ phase group with rhombohedra structure without any impurities [26, 28]. The refined parameters are χ^2 (goodness fit) = 1.19 and weighted refined parameter (wRp) = 0.05. Table 1 displays the fractional coordinates and the occupancies. Table 2 displays the bond vectors with their bond lengths and bond angle with atom coordinates, respectively. The calculated lattice parameters a , b and c values are 5.480 Å, 5.480 Å and 13.47 Å (± 0.002 Å), respectively [29, 30].

Figure 1b displays the Raman spectroscopy of NBTO powders obtained at room temperature (RT). A and E of transverse (TO) modes and longitudinal (LO) vibration modes are evident from the spectra [31, 32]. At room temperature, NBTO crystallize with rhombohedra $R3C$ phase and the factor group analysis showed the yields at $4A_1 + 9E$ optical modes [32]. The peaks at 142.85 cm^{-1} , 276.38 cm^{-1} and 569.65 cm^{-1} are where the low-frequency band is allied with the Na–O bonds and likely the higher-frequency bands are assigned to vibrations at the TiO_6 (octahedral). The bismuth element has higher mass (208.9804 u ± 0.00001 u) when compared to other elements in the perovskite structure. It has been reported that the mode corresponding to the Bi–O band would appear at low frequencies. Bi–O band has not been observed in any of the experimental conditions [33]. Figure 1c shows the SEM images of NBTO captured at RT, which clearly shows the

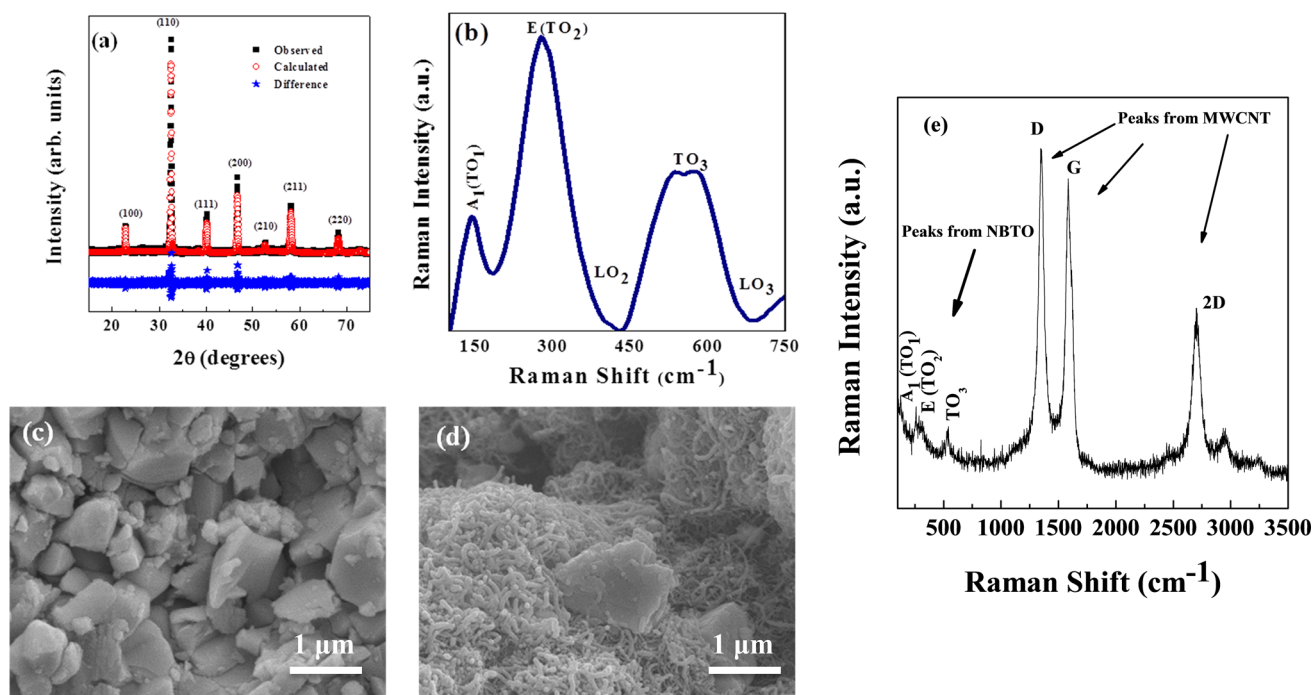


Figure 1 **a** Rietveld refined XRD pattern of NBTO perovskite material. **b** The Raman spectra of NBTO recorded at room temperature. **c** SEM analysis of NBTO captured at room temperature proves the layered structure and micron size of the

material. **d** SEM analysis of NBTO mixed with CNT. **e** The Raman spectra of NBTO/CNT composite recorded at room temperature.

Table 1 Equivalent atomic positions of $\text{Na}_{0.5}\text{Bi}_{0.5}\text{TiO}_3$ with thermal factor

S. no.	Name of the element	Fractional coordinates			Occupancy	Thermal factor
		<i>x</i>	<i>Y</i>	<i>Z</i>		
1	Na	0.0000	0.0000	1.2354	0.50	0.8000
2	Bi	0.0000	0.0000	0.3084	0.50	0.0489
3	Ti	0.0000	0.0000	0.0465	1.00	0.0169
4	O	0.1013	0.2903	0.1512	1.00	0.0083

randomly oriented micron size particles. Figure 1d shows the NBTO powder mixed with CNT, where the presence of NBTO as well as CNT is clearly seen. Figure 1e displays the Raman spectra of NBTO/CNT composite obtained at RT. Raman modes corresponding to both NBTO and MWCNTs are seen to be present. D, G and 2D bands from MWCNTs appear due to the amount of disorder in the nanotubes, degree of nanotubes graphitization and the stresses, respectively.

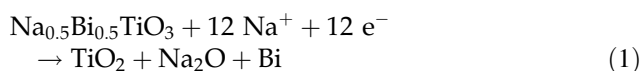
To explore the electrochemical performance of NBTO as an anode material for sodium ion batteries, electrochemical properties of NBTO material are measured and presented in Fig. 2. To investigate the sodium storage mechanism, cyclic voltammogram was carried out with a sweep rate of 0.1 mV s^{-1}

between 0.01 and 3 V voltage region (Fig. 2a). The reduction and oxidation scan represents the sodiation and desodiation processes. During the first cathodic scan, NBTO shows broad peaks between 0.8 and 0.2 V, attributed to SEI layer formation during the first cycle. During the subsequent cycles, it disappears and the CV curves show peak around $\sim 0.62 \text{ V}$ and 0.35 V , associated with conversion and alloying reactions of NBTO on sodium insertion. Likewise, during the consecutive anodic scan, two redox peaks are observed at 0.69 V and 0.8 V attributed to sodium removal process following the sodium insertion. During the first discharge, the whole perovskite structure of NBTO is destroyed, which was observed through the ex situ XRD and XPS measurements (discussed latter).

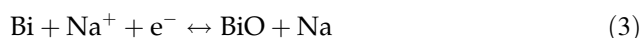
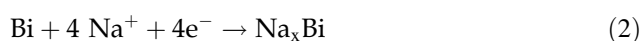
Table 2 Structural details observed through Rietveld refinement of Na_{0.5}Bi_{0.5}TiO₃—XRD pattern

Bond	Bond length (Å)	Atom coordinates			Bond angles (°)
		X	Y	Z	
Na–Na	3.881	– 0.666	– 0.333	1.402	–
Bi–Na	0.982	0.000	0.000	0.235	Bi–Na–Bi &
Na–Bi	0.982	0.000	0.000	1.308	Na–Bi–Na (111.766)
Bi–Na	0.982	0.000	0.000	0.235	Bi–Na–Ti (180.000)
Na–Ti	2.546	0.000	0.000	1.046	
Bi–Na	0.982	0.000	0.000	0.235	Bi–Na–O (129.080)
Na–O	1.801	0.101	0.290	1.151	
Bi–Ti	3.528	0.000	0.000	0.046	–
Na–O	1.801	0.101	0.290	1.151	Na–O–Bi (17.486)
O–Bi	2.538	0.000	0.000	0.308	
Ti–Na	2.546	0.000	0.000	0.235	Ti–Na–Ti &
Na–Ti	2.546	0.000	0.000	1.046	Na–Ti–Na (84.584)
Ti–Bi	3.528	0.000	0.000	0.308	–
Na–Ti	2.546	0.000	0.000	1.046	Na–Ti–O (44.766)
Ti–O	1.986	0.101	0.290	0.151	
O–Na	1.801	0.000	0.000	0.235	O–Na–O (84.484)
Na–O	1.801	0.101	0.290	1.151	Na–O–Na (115.703)
O–Bi	2.538	0.000	0.000	0.308	O–Bi–O (57.000)
Bi–O	2.538	0.101	0.290	0.151	Bi–O–Bi (100.417)
O–Ti	1.986	0.000	0.000	0.046	O–Ti–O (75.159)
Ti–O	1.986	0.101	0.290	0.151	
Ti–Na	2.546	0.000	0.000	0.235	Ti–Na–O (50.920)
Na–O	1.801	0.101	0.290	1.151	
Na–Bi	0.982	0.000	0.000	1.308	Na–Bi–O (33.434)
Bi–O	2.538	0.101	0.290	0.151	
Na–O	1.801	0.101	0.290	1.151	Na–O–Ti (84.315)
O–Ti	1.986	0.000	0.000	0.046	
Bi–O	2.538	0.101	0.290	0.151	Bi–O–Ti (101.800)
O–Ti	1.986	0.000	0.000	0.046	

With respect to observed cyclic voltammetry, the chemical reactions can be expressed with the conversion redox mechanism;



The cyclic voltammetry shows two distinguished peaks in charge and discharge phases of the cycle, which is clearly displayed in Fig. 2a. This may be due to the two stage alloying process between Na and Bi. This confirms the conversion reaction and disintegration of the perovskite structure [31].



Galvanostatic cycling in the voltage window of 0.001–3 V versus Na/Na⁺ was carried out to study

the cycling behavior NBTO anode. Figure 2b shows the charge–discharge voltage profile of NBTO anode for first five cycles at the current density of 100 mA g^{−1}. The charge/discharge profile at 100 mAh g^{−1} (Fig. 3a) shows a first cycle discharge capacity of ~ 1565 mAh g^{−1} and charge capacity of ~ 398 mAh g^{−1}, corresponding to a columbic efficiency of ~ 26%. This low columbic efficiency is attributed mainly to the solid electrolyte interface (SEI) layer formation at lower voltage. Despite the low columbic efficiency, it increases with cycling, and columbic efficiency reaches ~ 99% in few cycles. The discharge profile shows two plateaus at ~ 0.64 and 0.34 V, and the charge profile shows two plateaus at ~ 0.68 V and 0.82 V, and the shape profile is in correlation with CV studies. The NBTO retained a good discharge capacity stabilized from 5th cycle

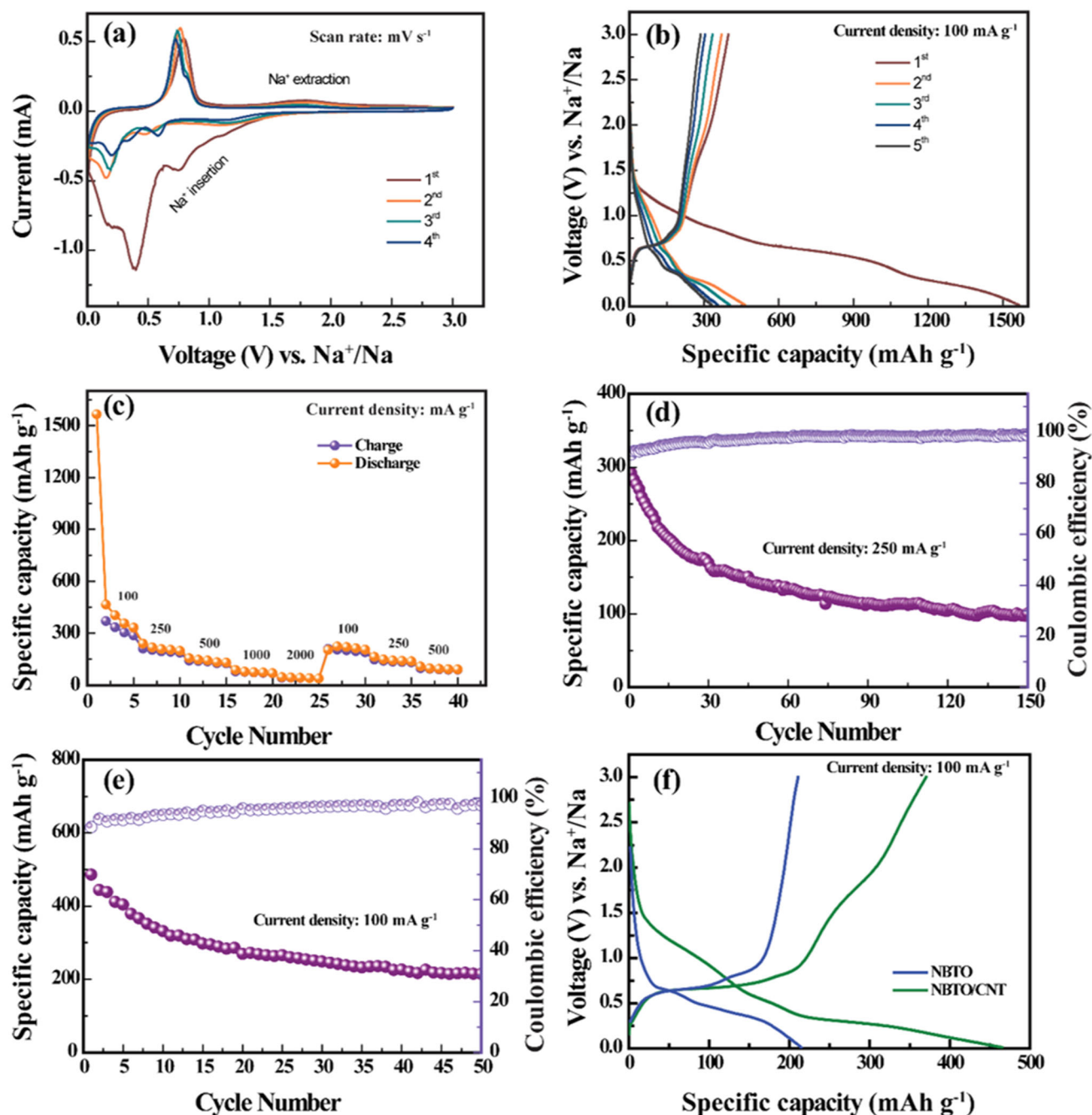


Figure 2 Electrochemical performance of NBTO anode for sodium ion batteries. **a** Cyclic voltammogram of NBTO anode at scan rate of 0.1 mV s^{-1} versus Na/Na^+ . **b** Charge–discharge voltage profile of NBTO anode at current density of 100 mA g^{-1} . **c** Rate performance of NBTO anode. **d** Cycling performance of

with a discharge capacity of $\sim 331 \text{ mAh g}^{-1}$. To explore rate behavior of the NBTO anode, the half-cell was tested at different current densities ranging from 100 to 2000 mA g^{-1} (Fig. 2c) and corresponding charge–discharge profiles shown in Fig. 2c. The

NBTO anode at current density of 250 mA g^{-1} . **e** Cycling performance of NBTO anode at current density of 100 mA g^{-1} . **f** Second charge/discharge curve of NBTO and NBTO/CNT at 100 mA g^{-1} .

discharge capacities at the current density of 100, 250, 500, 1000 and 2000 mA g^{-1} were 467, 240, 153, 90 and 52 mAh g^{-1} , respectively (Table 3). At second cycle, $\text{Na}_{0.5}\text{Bi}_{0.5}\text{TiO}_3$ delivers a high capacity of $\sim 470 \text{ mAh g}^{-1}$ at 100 mA g^{-1} (Fig. 2e) and 230 mAh g^{-1} at

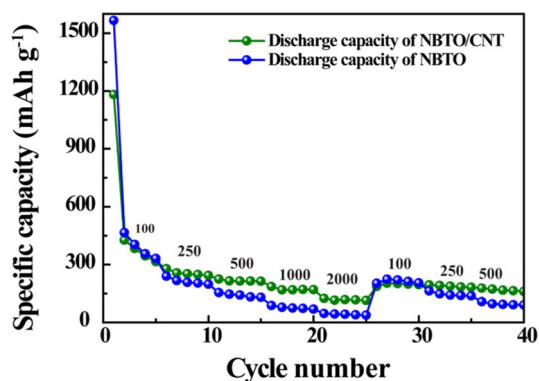


Figure 3 Rate performance of NBTO/CNT and NBTO anode at various C rates.

250 mA g⁻¹. Further, the electrode delivered a capacity of 237 mAh g⁻¹ when the current of decreased to 100 mA g⁻¹ after cycling at high current density of 2000 mA g⁻¹. These results are indicating good rate performance of NBTO as anode for sodium ion batteries. The cycling performance of NBTO anode is shown in Fig. 2d. After 50 cycles, the NBTO anode delivers a capacity of 215 mAh g⁻¹ at the current density of 100 mA g⁻¹. Coulombic efficiencies (charge capacity/discharge capacity) of around 98% is observed for the NBTO anode electrode during the entire 50 cycles, except the very few cycles. This demonstrates the good cycling performance of NBTO perovskite as anode for sodium ion batteries. In order to vary the CNT percentage and check the performance of NBTO, the electrochemical performance of NBTO anode without CNT (0% CNT) was fabricated and characterized. Figures 2f and 3 show the electrochemical performance of cells with and without CNT. At second charge and discharge, the reversible capacity of NBTO/CNT (465 mAh g⁻¹) anode is higher as compared to NBTO (215 mAh g⁻¹) without CNT (0% CNT). Discharge capacity of NBTO/CNT composite exhibits high capacity at various C rates compared to the bare NBTO electrode, which indicates that CNT can improve the

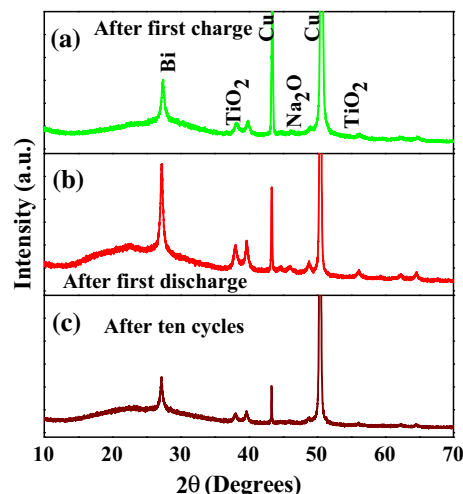


Figure 4 Ex situ XRD analysis of NBTO anode material. (a) After first charge, (b) after first discharge, (c) ten full cycles of charge and discharge.

conductivity of composite and thereby enhances the utilization efficiency of the NBTO anode.

In order to probe the changes in oxidation state of metal, oxygen ions and the crystal structure, ex situ XRD and XPS characterizations are carried out on the cycled NBTO electrodes. After completion of first discharge, first cycle and ten full electrochemical cycles, coin cells containing NBTO electrodes were opened in Ar-filled glow box to get the reacted NBTO electrodes. Electrochemically reacted electrodes were dried inside the glow box for 1 day and sealed in an Ar-filled box. Sealed electrodes were carried to the XRD and XPS measurements, and the experiments were performed immediately to avoid any reaction with atmosphere. Figure 4 shows the ex situ XRD analysis of the NBTO electrodes after first discharge, first charge and 10 full cycles. After first discharge, NBTO rhombohedral structure is totally destroyed and it contains Bi, TiO₂ and Na₂O phases. Cu peaks are observed because the slurry was coated on the copper foil, which was used as a NBTO electrode in the coin cell. Ex situ XRD pattern of NBTO electrodes

Table 3 Specific discharge capacity of Na_{0.5}Bi_{0.5}TiO₃ at different current rates

Current density (mA g ⁻¹)	Number of cycles (Nos.)	Discharging capacity (mAh g ⁻¹)	Efficiency (%)
250	50	141	99
100	50	215	98

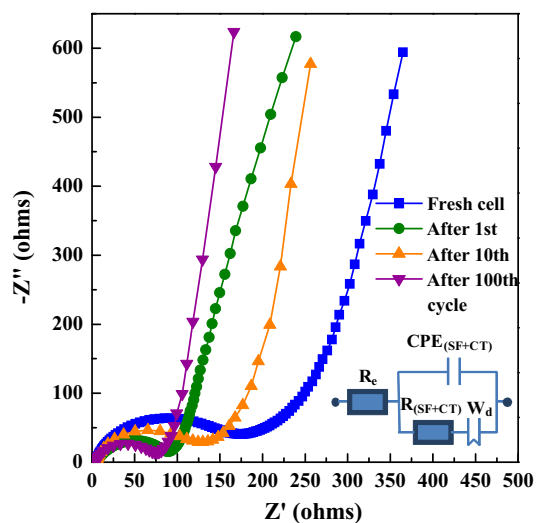


Figure 5 Electrochemical impedance spectra of NBTO anode before and after cycling.

after first charge and 10th cycle also contains Bi, TiO_2 and Na_2O phases.

Figure 5 shows the electrochemical impedance spectra of NBTO cell with Na reference electrode. Measurements were carried out on a fresh cell and after completion of ten cycles. Impedance spectroscopy (IS) data was fit with an equivalent circuit consist of constant phase element (CPE), resistors such as liquid electrolyte resistance (R_e), charge transfer (CT) impedance $R_{(\text{SF}+\text{CT})}$, the surface layer film (SF) and Warburg element (W_d) [34]. It is shown in inset of Fig. 4. Nyquist plot clearly shows depressed semicircles at high frequencies and an inclined straight line at low frequencies for both cells. Appearance of semicircle at high frequencies is due to the formation of thin layer at the surface which can transport the Na ions and the electrode/electrolyte interface charge transfer (CT). In the case of fresh cell, surface thin layer contribution depends on the concentration of liquid electrolyte. The inclined straight line at low frequency occurs due to the semi-infinite diffusion of the Na ions on the electrode system (R_e) [35–38]. Diameter or intercept of the semicircle with x-axis for the fresh cell is seen to be higher than that of the cycled cell due to the decrement of R_f and R_{ct} resistance as the cycle number increases [38]. This phenomenon was explained by Song et al. [36]. as the high surface area and structural defects of material, which leads to large irreversible ion insertion into the electrode with the cycle process, which in turn may be a lead to the increase of electrical conductivity. In

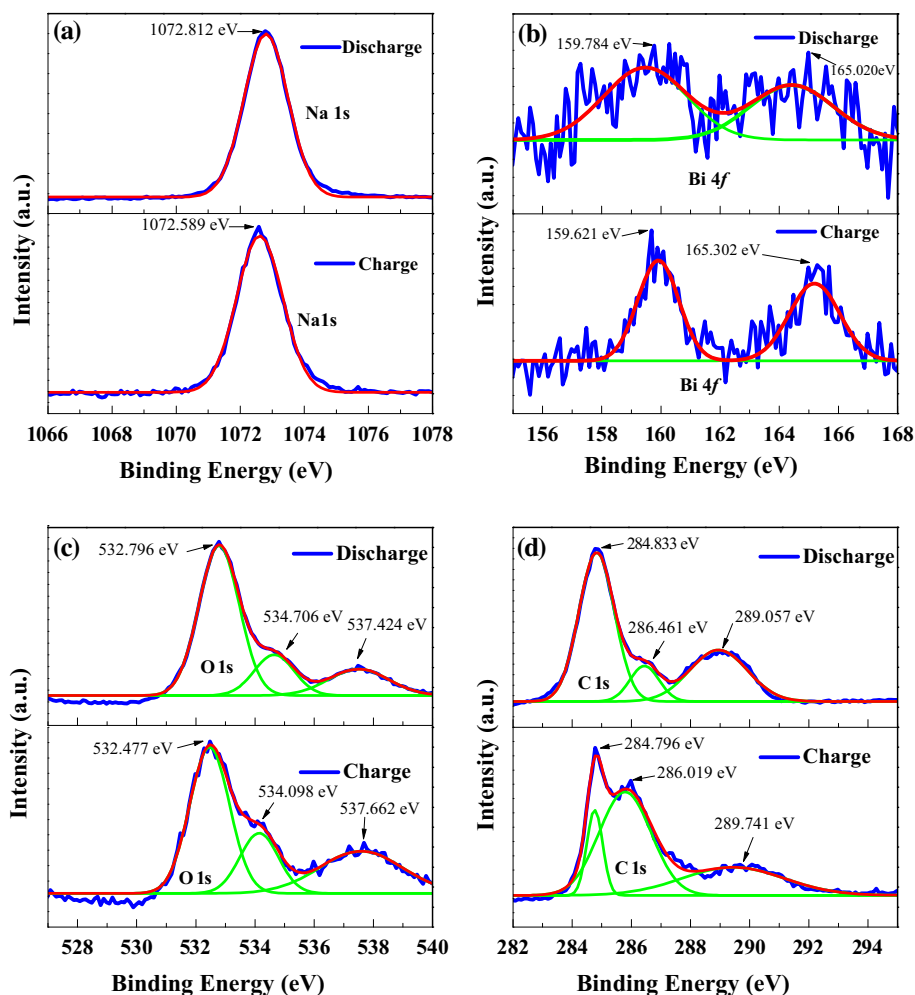
the present case, NBTO perovskite material is destroyed and metal oxide formation takes place after the first discharge. In addition to that, solid electrode interface (SEI) layer formation also affects the conductivity. Due to this the Na insertion into electrode becomes irreversible which finally, increases the electrical conductivity. Resistance after 100th cycle is seen to be lower than that of 10th cycle. Hence, it is very clear that the IS analysis are clearly supporting the conversion reaction mechanism in the NBTO perovskite anode material.

XPS analysis of the NBTO electrodes after first discharge and first charge were carried out and are shown in Fig. 6. Figure 6a shows the XPS spectra of sodium, (Na1s). The peak at ~ 1073 eV with some distortion (in the charging) and a fine peak at discharging prove the presence of Na in the NBTO electrodes. In additional to that, Na 1s peak confirms that the oxidation state of Na in NBTO was +1 [39]. Figure 6b shows the bismuth (Bi 4f) doublet peaks centered at ~ 159 eV and ~ 165 eV binding energies for both charge and discharge electrodes. High-resolution spectrum for Bi 4f state examined with peaks at 159 eV (± 1 eV) and 165 eV (± 1 eV) expressed the presence of bismuth in $4f_{7/2}$ and $4f_{5/2}$ states, respectively [40, 41]. Figure 6c shows the XPS peaks of oxygen (O 1s) compound in the NBTO electrode with peaks centered at ~ 532 eV, ~ 534 eV and ~ 537 eV. The binding energy of O1s at 531.3 eV (± 1 eV) can be a reason assigned to O=C and at 533.1 eV (± 1 eV) is the peak which corresponds to O–C bonds [42], at charging and discharging phases. The peak at 537 eV is referred as the emergence of shake up satellite in O 1s spectra of occupied and vacant orbitals of O–O bonds [43]. XPS spectra of carbon (C 1s) is shown in Fig. 6d which has the distinguished peaks identified at binding energies ~ 284 eV, ~ 286 eV and ~ 289 eV. Through this, the presence of C–C, C–O and C=O bonds was confirmed [44]. The peak at ~ 286 eV has an intensity variation for the discharged and charged electrodes, supported with the change in intensity of C–O bonds formations [44] on the process of charging and discharging.

Conclusion

In this work, pure $\text{Na}_{0.5}\text{Bi}_{0.5}\text{TiO}_3$ perovskite material was successfully prepared by solid-state reaction method and tested as an anode material for sodium

Figure 6 XPS analysis of cycled NBTO anode after first discharge and first charge. a Na 1s, b Bi 4f, c O 1s d C 1s.



ion batteries. The crystal structure and morphological properties of as prepared $\text{Na}_{0.5}\text{Bi}_{0.5}\text{TiO}_3$ bulk material were examined by XRD, Raman spectroscopy and SEM techniques. This material delivers a high capacity of $\sim 470 \text{ mAh g}^{-1}$ at 100 mA g^{-1} and 230 mAh g^{-1} at 250 mA g^{-1} when it is mixed with MWCNT. The material exhibits a capacity of 215 mAh g^{-1} after 50 cycles at current density of 100 mA g^{-1} . Further, electrochemical redox process during the charge/discharge cycles was investigated using ex situ XRD and XPS measurements. Hence, this study proposes $\text{Na}_{0.5}\text{Bi}_{0.5}\text{TiO}_3$ perovskite can be employed as an anode material for Na ion batteries after stabilizing the capacity fading effect.

Compliance with ethical standards

Conflict of interest As a corresponding author, on behalf of all the authors I am declaring that the article is original. The article has been written by the stated

authors who are all aware of its content and approve its submission. The article has not been published previously. The article is not under consideration for publication elsewhere. No conflict of interest exists. If accepted, the article will not be published elsewhere in the same form, in any language, without the written consent of the publisher.

References

- [1] Li X, Kehui Q, Yuyan G, Xia H, Fangdong Z (2015) High potential performance of Cerium-doped $\text{LiNi}_{0.5}\text{Co}_{0.2}\text{Mn}_{0.3}\text{O}_2$ cathode material for Li-ion battery. *J Mater Sci* 50:2914–2920. <https://doi.org/10.1007/s10853-015-8856-9>
- [2] Johnston-Peck AC, Takeuchi S, Bharathi KK, Herzing AA, Bendersky LA (2018) Local degradation pathways in lithium-rich manganese–nickel–cobalt oxide epitaxial thin films. *J Mater Sci* 53:1365–1379. <https://doi.org/10.1007/s10853-017-1593-5>

- [3] Aricò AS, Bruce P, Scrosati B, Tarascon JM, Schalkwijk WV (2005) Nanostructured materials for advanced energy conversion and storage devices. *Nat Mater* 4:366–377
- [4] Armand M, Tarascon JM (2008) Building better batteries. *Nature* 451:652–657
- [5] Thackeray MM, Wolverton C, Isaacs ED (2012) Electrical energy storage for transportation—approaching the limits of, and going beyond, lithium-ion batteries. *Energy Environ Sci* 5:7854–7863
- [6] Vetter J, Novak P, Wagner MR, Veit C, Moller KC, Besenhard JO, Winter M, Mehrens MW, Vogler C, Hammouche A (2005) Ageing mechanisms in lithium-ion batteries. *J Power Sources* 147:269–281
- [7] Friege H, Reutter L, Gnutzmann N, Klöffer A, Mohrlök M, Sauce ADL, Wons W, Kross S (2016) An examination of batteries remaining in used electric and electronic devices: insights gained from a trans disciplinary project. *Recycling* 1:321–327
- [8] Kim SM, Seo DH, Ma X, Ceder G, Kang K (2012) Electrode materials for rechargeable sodium-ion batteries: potential alternatives to current lithium-ion batteries. *Adv Energy Mater* 2:710–721
- [9] Kim D, Kang SH, Slater M, Rood S, Vaughey JT, Karan N, Balasubramanian M, Johnson CS (2011) Enabling sodium batteries using lithium-substituted sodium layered transition metal oxide cathodes. *Adv Energy Mater* 1:333–336
- [10] Ko YN, Choi SH, Kang YC (2016) Hollow cobalt selenide microspheres: synthesis and application as anode materials for Na-ion batteries. *ACS Appl Mater Interfaces* 8:6449–6456
- [11] Jache B, Adelhelm P (2014) Use of graphite as a highly reversible electrode with superior cycle life for sodium-ion batteries by making use of Co-intercalation phenomena. *Angew Chem Int Ed* 53:10169–10173
- [12] Ji L, Lin Z, Alcoutlabi M, Zhang X (2011) Recent developments in nanostructured anode materials for rechargeable lithium-ion batteries. *Energy Environ Sci* 4:2682–2699
- [13] Wu HB, Chen JS, Hng HH, Lou XW (2012) Nanostructured metal oxide-based materials as advanced anodes for lithium-ion batteries. *Nanoscale* 4:2526–2542
- [14] Goriparti S, Miele E, Angelis FD, Fabrizio ED, Zaccaria RP, Capiglia C (2014) Review on recent progress of nanostructured anode materials for Li-ion batteries. *J Power Sources* 257:421–443
- [15] Tian H, Xin F, Wang X, He W, Han W (2015) High capacity group-IV elements (Si, Ge, Sn) based anodes for lithium-ion batteries. *J Materiomics* 1(3):153–169
- [16] Yu L, Wang LP, Xi S, Yang P, Du Y, Srinivasan M, Xu ZJ (2015) β -FeOOH: an earth-abundant high-capacity negative electrode material for sodium-ion batteries. *Chem Mater* 27(15):5340–5348
- [17] Jiang Y, Hu M, Zhang D, Yuan T, Sun W, Xu B, Yan M (2014) Transition metal oxides for high performance sodium ion battery anodes. *Nano Energy* 5:60–66
- [18] Sun Q, Ren QQ, Li H, Fu ZW (2011) High capacity Sb₂O₄ thin film electrodes for rechargeable sodium battery. *Electrochem Commun* 13:1462–1464
- [19] Hu Z, Wang LX, Zhang K, Wang JB, Cheng FY, Tao ZL, Chen J (2014) MoS₂ nanoflowers with expanded interlayers as high-performance anodes for sodium-ion batteries. *Angew Chem Int Ed* 53:12794–12798
- [20] Shimizu M, Usui H, Sakaguchi H (2014) Electrochemical Na insertion/extraction properties of SnO thick-film electrodes prepared by gas-deposition. *J Power Sources* 248:378–382
- [21] Xu J, Wang M, Wickramaratne NP, Jaronie M, Dou S, Dai L (2015) High-performance sodium ion batteries based on three-dimensional anode from nitrogen-doped graphene foams. *Adv Mater* 27:2042–2048
- [22] Ponrouch A, Goñi AR, Palacín MR (2013) High capacity hard carbon anodes for sodium ion batteries in additive free electrolyte. *Electrochem Commun* 27:85–88
- [23] Pol VG, Lee E, Zhou D, Dogan F, Calderon-Moreno JM, Johnson CS (2014) Spherical carbon as a new high-rate anode for sodium-ion batteries. *Electrochim Acta* 127:61
- [24] Veerappana G, Yoo S, Zhang K, Ma M, Kang B, Park JH (2016) High-reversible capacity of perovskite BaSnO₃/rGO composite for lithium-ion battery anodes. *Electrochim Acta* 214:31–37
- [25] Sharma Y, Sharma N, Subba Rao GV, Chowdari BVR (2008) Studies on nano-CaO-SnO₂ and nano-CaSnO₃ as anodes for Li-ion batteries. *Chem Mater* 20(21):6829–6839
- [26] Jones GO, Thomas PA (2002) Investigation of the structure and phase transitions in the novel A-site substituted distorted perovskite compound Na_{0.5}Bi_{0.5}TiO₃. *Acta Cryst B* 58:168–178
- [27] Dorcet V, Trolliard G, Boullay P (2008) Reinvestigation of phase transitions in Na_{0.5}Bi_{0.5}TiO₃ by TEM. Part I: first order rhombohedral to orthorhombic phase transition. *Chem Mater* 20:5061–5073
- [28] Ranjan R, Dviwedi A (2005) Structure and dielectric properties of (Na_{0.50}Bi_{0.50})_{1-x}Ba_xTiO₃: 0 ≤ x ≤ 0.10. *Solid State Commun* 135:394–399
- [29] Ge W, Luo C, Zhang Q, Ren Y, Li J, Luo H, Viehland D (2014) Evolution of structure in Na_{0.5}Bi_{0.5}TiO₃ single crystals with BaTiO₃. *Appl Phys Lett* 105:1629131-5
- [30] Kaswan K, Agarwal A, Sanghi S, Singh O (2015) Rietveld refinement and dielectric properties of (Na_{0.5}Bi_{0.5}TiO₃)–

- ($\text{Bi}_{0.8}\text{Ba}_{0.2}\text{FeO}_3$) ceramics. In: AIP conference proceedings, vol 1665, p 140014
- [31] Lignesh D, Brindha M, Thomas CI, Kim DK, Bharathi KK (2017) Electrochemical properties of BiFeO_3 nanoparticles: anode material for sodium-ion battery application. *Mater Sci Semicond Process* 68:165–171
- [32] Suchanicz J, Sumara IJ, Kruzina TV (2011) Raman and infrared spectroscopy of $\text{Na}_{0.5}\text{Bi}_{0.5}\text{TiO}_3$ – BaTiO_3 ceramics. *J Electroceram* 27:45–50
- [33] Saïd S, Marchet P, Merle-Méjean T, Mercurio JP (2004) Raman spectroscopy study of the $\text{Na}_{0.5}\text{Bi}_{0.5}\text{TiO}_3$ – PbTiO_3 system. *Mater Lett* 58:1405–1409
- [34] Kumar PR, Jung YH, Bharathi KK, Lim CH, Kim DK (2014) High capacity and low cost spinel Fe_3O_4 for the Na-ion battery negative electrode materials. *Electrochim Acta* 146:503–510
- [35] Hu L, Zhong H, Zheng X, Huang Y, Zhang P, Chen Q (2012) CoMn_2O_4 spinel hierarchical microspheres assembled with porous nanosheets as stable anodes for lithium-ion batteries. *Sci Rep* 2(986):1–8
- [36] Song R, Song H, Zhou J, Chen X, Wua B, Yang HY (2012) Hierarchical porous carbon nanosheets and their favorable high-rate performance in lithium ion batteries. *J Mater Chem* 22:12369
- [37] Yang S, Song H, Chen X, Okotrub AV, Bulusheva LG (2007) Electrochemical performance of arc-produced carbon nanotubes as anode material for lithium-ion batteries. *Electrochim Acta* 52:5286–5293
- [38] Ruffo R, Fathi R, Kim DJ, Jung YH, Mari CM, Kim DK (2013) Impedance analysis of $\text{Na}_{0.44}\text{MnO}_2$ positive electrode for reversible sodium batteries in organic electrolyte. *Electrochim Acta* 108:575–582
- [39] Li M, Zhang LL, Yang XL, Sun HB, Huang YH, Liang G, Nia CB, Tao HC (2015) Synthesis and electrochemical performance of Na modified $\text{Li}_2\text{Fe}_{0.5}\text{Mn}_{0.5}\text{SiO}_4$ cathode material for Li ion batteries. *RSC Adv* 5:22818–22824
- [40] Bhunia H, Bar A, Bera A, Pal AJ (2017) Simultaneous observation of surface- and edge-states of a 2D topological insulator through scanning tunneling spectroscopy and differential conductance imaging. *Phys Chem Chem Phys* 19:9872–9878
- [41] Perejon A, Jimenez PS, Maqueda LP, Criado JM, Paz JRD, Puche RS, Maso N, West AR (2014) Single phase, electrically insulating, multiferroic La-substituted BiFeO_3 prepared by mechanochemistry. *J Mater Chem C* 2:8398–8411
- [42] Wu M, Feng Q, Sun X, Wang H, Gielen G, Wu W (2015) Rice (*Oryza sativa* L.) plantation affects the stability of biochar in paddy soil. *Sci Rep* 5:10001
- [43] Stadnichenko AI, Koshcheev SV, Boronin AI (2007) Oxidation of the polycrystalline gold foil surface and XPS study of oxygen states in oxide layers. *Mosc Univ Chem Bull* 62(6):343–349
- [44] Sun T, Zhang Z, Xiao J, Chen C, Xiao F, Wang S, Liu Y (2013) Facile and green synthesis of palladium nanoparticles-graphene-carbon nanotube material with high catalytic activity. *Sci Rep* 3:2527

Publisher's Note Springer Nature remains neutral with regard to jurisdictional claims in published maps and institutional affiliations.